Available online at www.sciencedirect.com
ScienceDirect
Journal of Molecular Graphics and Modelling 26 (2007) 48–61
Journal of Molecular Graphics and Modelling
www.elsevier.com/locate/JMGM

Modelling and study of cyclosporin A and related compounds in complexes with a *Trypanosoma cruzi* cyclophilin

Roberto Carraro [a], Jacqueline Búa [b], Andrés Ruiz [b], Margot Paulino [a,*]

[a] *Physical Chemistry and Mathematics Department, Molecular Pharmacology and Biomodelling Laboratory, Facultad de Química, Universidad de la República, General Flores 2124, 11800 Montevideo, Uruguay*
[b] *Instituto Nacional de Parasitología Dr. M. Fatala Chabén, Av. Paseo Colón 568 (1063), ANLIS, C.G. Malbrán, Buenos Aires, Argentina*

Received 10 March 2006; received in revised form 8 September 2006; accepted 20 September 2006
Available online 26 September 2006

Abstract

Cyclophilins (CyPs) are enzymes involved in protein folding, catalyzing the isomerisation of peptidyl prolyl bonds in proteins and peptides between the *cis*- and *trans*-conformations. They are also the major cellular target for the immunosuppressive drug Cyclosporin A (CsA). In *Trypanosoma cruzi*, the most abundantly expressed CyP is an isoform of 19 kDa, *Tc*CyP19, in which the enzymatic activity is inhibited by CsA. Among a reported set of CsA analogues, two non-immunosuppressive compounds, H-7-94 and F-7-62, proved to be the best inhibitors of *Tc*CyP19 enzymatic activity as well as the most efficient trypanocidal drugs.

With the objective of analysing, at the molecular level, how the structural differences between the three above-mentioned inhibitors justify their different inhibitory activity on *Tc*CyP19, three-dimensional molecular modelling structures were generated to computationally simulate behaviours and interactions. An energy-minimized model of each binary complex in water with ions was obtained. These models were then used as starting point for molecular dynamic simulations, performed with GROMOS96 program.

With the resulting set of co-ordinates and energies, a comparison of the interaction between CsA and both CsA analogues in *T. cruzi* and human cyclophilins were performed. Within the different magnitudes analysed, the total potential complex energy exhibited the best correlation with the experimental data.

The results obtained in this study support the use of this methodology when designing new lead inhibitor compounds.

Keywords: *Trypanosoma cruzi*; Cyclophilins; Cyclosporin A analogues; Chagas' disease chemotherapy; Molecular modelling; Molecular dynamic simulations

1. Introduction

Chagas' disease is caused by the protozoon *Trypanosoma cruzi*, and it is still an important health problem in America. The cause, among others, is that the chemotherapy with available drugs with a similar structure and presumably similar mode of action, limited efficacy and similar toxicity profile (Nifurtimox® and Benznidazol®), cannot be rated as satisfactory [1,2].

Cyclophilins (CyPs) are cyclosporin A (CsA) binding proteins [3], which catalyze the isomerisation between *cis*- and *trans*-conformations of peptidyl proline bonds in peptides or proteins (PPIase activity) [4]. PPIases are involved in protein folding, and they interact with many proteins that control diverse cellular processes (reviewed in [5]). The hCyP18–CsA complex binds to the serine/threonine phosphatase calcineurin [6], interfering with the expression of cytokines in T cells, leading immunosuppression, for which CsA, a cyclic undecapeptide, is used in human organ therapeutic transplantation [7].

The *T. cruzi* genome encodes 15 cyclophilin paralogues and this *T. cruzi* CyP gene family has been classified. Some members belong to the previously established cyclophilin classes whereas some others display less defined patterns of their protein sequence attributes [8].

The most abundantly expressed cyclophilin at the *T. cruzi* epimastigote stage is *Tc*CyP19, a 19 kDa cyclophilin, which accounts for roughly 60% of the retained CsA-affinity chromatography proteins. *Tc*CyP19 exhibit a CsA-sensitive

* Corresponding author. Tel.: +598 2 929 1558; fax: 598 2 924 7697.
E-mail address: margot@fq.edu.uy (M. Paulino).

1093-3263/$ – see front matter
doi:10.1016/j.jmgm.2006.09.008

PPIase activity [9]. CsA displays anti-parasitic activity in protozoans [10], including *T. cruzi* [11] and helmints. We have shown that some non-immunosuppressive CsA derivatives exhibited a potent anti-*T. cruzi* activity *in vitro* without toxic effects on mammalian cells, interfering as well with the PPIase activity of *Tc*CyP19 [12]. Two out of eight CsA analogs, H-7-94 and F-7-62, exhibited the most efficient anti-parasitic action on all *T. cruzi* stages studied. Their IC_{50} values were 0.82 and 3.41 μM, respectively, compared to CsA IC_{50} value 5.39 μM on epimastigote proliferation. These drugs also showed a more efficient trypomastigote lysis with an IC_{50} of 0.97 and 2.66 μM, respectively, than CsA IC_{50}, 7.19 μM. With regards to inhibition *Tc*CyP19 enzymatic activity, these analogs were also the best (IC_{50} = 12.54, 13.30, 14.42 nM, for H-7-94, F-7-62 and CsA, respectively) [12].

*Tc*CyP19 is the most expressed cyclophilin in the parasite and H-7-94 and F-7-62 proved to be the best trypanocidal drugs. Taking into account that the structural difference between the CsA, H-7-94 and F-7-62 is located in the side-chain of the first residue (MeBmt in CsA), it remains the question of how these changes drove the different activities. An approach to contribute in the answering of this question was the use of complexed three-dimensional-structures and all available graphical and computational resources to simulate behaviours and to sense interaction energies. The use of computational and graphical tools applied to research in the pharmacology and or molecular biology, as it is the case of the work under investigation, is a very common and complementary way to give answers when the experiments are not available, too expensive or unfeasible.

In this report, we have used homology modelling and other computer-assisted-modelling techniques to obtain the three-dimensional-structure of the *Tc*Cyp19–CsA (and analogues) complexes. This procedure has become an extremely useful technique to predict three-dimensional structures [13] and it has allowed us to make a sampling for conformational and energetic evaluations [14–17]. In addition, we show a molecular model of a mutant protein, named CyPM, in which a phenylalanine has substituted the tryptophan at the residue 121 of hCyP18. This protein, obtained by genetic engineering, had 75-fold decreased sensitivity to CsA while rotamase activity drops only 2-fold. [33]. A change in just one residue, with the loss of one H-bond (that of Trp121) is enough to cause a sharp drop in the activity. Moreover, in the absence of H-7-94 and F-7-62 hCyP18 inhibition data, the analysis of CsA–CyPM complex could be useful to predict unavailable data as well as for the understanding of action mechanisms of CsA and related, justifying the use of this protein as a model to understand the molecular basis of ligand–protein interactions under study.

2. Methodology

2.1. Sequence alignments

With the aim of finding an adequate template for homology modelling of *Tc*CyP19 and CyPM, sequence alignments of its amino acid sequence against Protein Data Bank (PDB [18]) were performed by means of the BLAST algorithm [19]. Finally, an alignment between the selected templates and the *Tc*CyP19 or the mutant CyPM was performed using the Needle global alignment program [20].

2.2. Molecular model building

The Nest module of the Jackal program [21] was used for obtaining the primary model of *Tc*CyP19 or CyPM, with the following relevant options: all the library rotamers were considered, only clash between atoms were eliminated and only insertion or deletion zones were minimized by means of three rounds of the minimization procedure. To obtain the co-ordinates of the cyclosporin analogues, the building and geometric optimisation facilities of the HyperChem 6.0 package [22] were used, taking as a template a conformer of Cyclosporin A bound to the cyclophilin available in the PDB database. The complex models (CsA or analogues with hCyP18 or *Tc*CyP19 and CsA–CyPM) were obtained by merging the coordinate files of modelled protein and ligands. A graphical inspection and control of possible atom clashes of the different models was performed by means of the of Swiss-PdbViewer program [23].

2.3. Molecular model refinement

All simulations were performed by means of the utilities of the GROMOS96 package using the 43A1 force field [24].

A truncated octahedron box with the SPC water model [25] and ions (Na^+ and Cl^-) was built. The box model, first with explicit water and then with ions, was submitted to 50 rounds of energy minimization, using the steepest descent algorithm with periodic conditions and restraining the solute (i.e. the protein and the corresponding ligand). The selected relevant options were: an initial step of 0.01 nm and a maximum step of 0.05 nm; a constraining of all bond lengths using SHAKE [26] procedure with a relative geometric tolerance of 0.0001; a pair list construction for atomic non-bonded interactions was performed with a 0.8 nm cut-off radii and updated every 10 steps. The long-range interactions were evaluated up to 1.4 nm; beyond 1.4 nm the electrostatic interactions were approximated by a Poisson–Boltzmann generalized reaction field. The minimization procedure stopped when the energy difference between two consecutive steps dropped below 0.1 kJ mol^{-1} or when 50 steps were reached. Then, a 5 ps solute restrained molecular dynamics procedure was performed with similar conditions as in Section 2.6. The refinement procedure was finished with a full energy minimization without any kind of restriction.

2.4. Evaluation of quality of refined molecular models

The quality of the refined models was carried out by means of their graphic display, the calculation of the root mean square deviations (rmsd) and the evaluation of the stereochemical parameters.

The graphic evaluation, made using Swiss-PdbViewer and VMD [27], allows a global visualization of all models, the comparison of secondary and tertiary structural differences between the model and the template molecule, and a quick visual inspection of distorted folding regions, breaks and bad contacts.

The calculation of the root mean square deviations (rmsd) was made between: (a) the different modelled protein chains and the crystallographic data used as template and (b) the modelled and crystallographic ligand co-ordinates.

The stereochemical parameters of the modelled polypeptidic chains were evaluated using Procheck V3.5 program analysis [28].

2.5. Analysis of the interaction between protein and ligands

To study the interaction between proteins and ligands, a list of contacting atoms at less than 3.7 Å was built by means of our own *ad hoc* programs and another list for the putative hydrogen bonds was built using the PROCHB program within the GROMOS package.

2.6. Molecular dynamics

Molecular dynamics simulations were performed over the resulting models of Section 2.3, with the purpose to obtaining a sample for conformational and energetic evaluations.

The models were submitted to molecular dynamics simulations up to 1000 ps. Initial velocities were assigned from a Maxwellian distribution at 300 K. All molecular dynamic simulations were performed according with the next parameters, using periodic conditions and the 43A1 force field implemented into GROMOS96 package. The time step integration was 2 fs. All bond lengths were constrained according to the SHAKE algorithm with a tolerance of 0.0001. A pair list was built before the first step, and updated each five steps with a cut-off of 1.2 nm. A cut-off of 1.4 nm was used for long-range interaction calculations and to calculate the reaction field correction. The temperature was kept constant at 300 K by coupling the system to a Berensen's thermal bath [29] with a coupling time of 0.1 ps. Co-ordinates and energy terms (total, kinetic and potential for the whole system, and electrostatic, distance-dependent, distance-independent reaction force field and Lennard–Jones for different interaction groups) were saved each picosecond.

2.7. Analysis of molecular dynamics

With the aim of evaluating the system stabilization throughout the molecular dynamics time, the total, kinetic and potential energy were plotted *versus* time. The stabilization was assessed by graphics visualization. In addition, for a more rigorous analysis, a *t*-test was performed over the data of simulations. The total energy averages over different time intervals from 100, 200, 300, 400, 500, 600, 700, 800 and 900 to 1000 ps were tested. A stable regime was assumed if the averages were not significantly different.

Different interesting energy terms were extracted by means of our own programs and were compared with experimental complex stability data.

First, the following total system energetic terms were evaluated: the total energy, the kinetic energy, the potential energy, the potential covalent energy and the potential non-covalent energy. The potential covalent energy is the potential energy calculated with force field functions associated to the covalent interactions (bond stretching, bond angle, proper and improper dihedral angle). The bond-stretching energies were specially treated with a geometric constraint (SHAKE) to save computing time. In the SPC rigid solvent model used by GROMOS, the solvent interactions are represented by non-covalent forces. Consequently, the potential covalent energy has no solvent contribution. The potential non-covalent energy includes the van der Waals and electrostatics terms.

Second, protein–ligand complex-related energetic terms were evaluated as the potential complex energy and the potential non-covalent complex energy. The potential complex energy was calculated by taking the total potential energy and deducting the potential energy of interaction between all the solvent molecules, the chlorine and the sodium ions. This value represents the energy due specifically to the protein–ligand interactions, excluding all intra-solvent (and ionic) influence. The same considerations are made for the calculation of potential non-covalent complex energy terms.

Third, energetic terms related to the ligands. The energy of binding of a ligand to a protein is generally calculated considering all interactions with protein contacting atoms (ligand–protein term in Table 7). In our calculations we included the interactions ligand–solvent (ligand–solvent), the ligand-surrounding (protein plus solvent) and the total non-covalent ligand energy (ligand-surrounding plus internal non-covalent energy of each ligand).

The protein and ligand atoms making contacts at less than 3.7 Å were analyzed by means of our own *ad hoc* programs (details are given in Section 3). The presumed hydrogen bonds were evaluated using the PROAHB program within the GROMOS package.

The molecular graphics analysis was performed by means of VMD and md-Frodo program [30].

3. Results and discussion

3.1. Sequence alignments

The search using the BLAST alignment algorithm within the PDB database showed various potential templates for molecular modelling purposes. More than 50 crystallographic structures were found showing high identity score with respect to *Tc*CyP19. When the root mean square difference for backbone atoms was calculated, they yielded values lower than 0.75 $Å^2$ in accordance with previous reports [31] and confirming that this is a highly conserved family of proteins. Unfortunately, on commencement of this work there were no crystallographic data about *T. cruzi* cyclophilins. However, there were crystallographic data about many CsA binary complexes with homologous cyclophilins, and

```
TcCyP19:          13  NPKVFFDVSIGGQSAGRVVFELFADAVPKTAENFRALCTGEKNFGYAGSGFHRIIPQFMC 72
                      NP VFFD+++ G+  GRV FELFAD VPKTAENFRAL TGEK FGY GS FHRIIP FMC
1m63(Chain C):     3  NPTVFFDIAVDGEPLGRVSFELFADKVPKTAENFRALSTGEKGFGYKGSCFHRIIPGFMC 62

TcCyP19:          73  QGGDFTNHNGTGGRSIYGEKFADESFAGKAGKHFGLGTLSMANAGPNTNGSQFFICTAPT 132
                      QGGDFT HNGTGG+SIYGEKF DE+F     KH G G LSMANAGPNTNGSQFFICTA T
1m63(Chain C):    63  QGGDFTRHNGTGGKSIYGEKFEDENF---ILKHTGPGILSMANAGPNTNGSQFFICTAKT 119

TcCyP19:         133  QWLDGKHVVFGQVLEGIEVVKAMEAVGSQTGKTSKPVKIEASGQL 177
                      +WLDGKHVVFG+V EG+ +V+AME  GS+ GKTSK + I   GQL
1m63(Chain C):   120  EWLDGKHVVFGKVKEGMNIVEAMERFGSRNGKTSKKITIADCGQL 164
```

Fig. 1. *Tc*CyP19 (target) and 1m63C (template) aligned sequences obtained by BLAST or Needle programs.

CsA ternary complexes with homologous cyclophilin and calcineurin. This allowed us to use homology modelling and other computer-assisted-modelling techniques to obtain the three-dimensional-structure of the *Tc*Cyp19–CsA (and analogues) complexes. It could be noted that the only published crystallographic data of a *T. cruzi* cyclophilin (*Tc*CyP21, 18 kDa, without the signal peptide, PDB codes 1XO7 and 1XQ7) has only 59% sequence identity with respect to *Tc*CyP19. Finally, the crystal structure of the human hCyP18 (PDB code: 1m63 (chain C)), a 2.8 Å resolution crystal structure of a calcineurin–cyclophilin–cyclosporin complex was selected because of its high sequence identity with *Tc*CyP19, an acceptable crystal resolution and the possibility to be used as a template to model binary as well as ternary complexes. The result of the aligned *Tc*CyP19 and 1m63 chain C (1m63C) is showed in Fig. 1.

The secondary structure of 1m63C chain is displayed in Fig. 2; it has 165 residues and 72% of sequence identity when compared to the 177 amino acids target protein. The catalytic residues are conserved in both proteins: R55, F60, M61, Q63, G72, A101, N102, A103, Q111, F113, W121, L122, H126 in 1m63C, and R65, F70, M71, Q73, G82, A114, N115, A116, Q124, F126, W134, L135, H139 for *Tc*CyP19 [32].

3.2. Modelling of binary complexes

The *Tc*CyP19 primary model obtained by means of Jackal program did not include the first 12 residues of the *Tc*CyP19 original sequence since we did not have an adequate template for them. So henceforth, the *Tc*CyP19 modelled sequence numbers started in fact in the residue 13 of the wild *Tc*CyP19 sequence. We think this limitation will not cause any problems in the model behaviour since this region is far from the CsA (or CsA analogues) binding site, according to the available crystallographic data.

The co-ordinates of the CsA analogues (Fig. 3) were obtained using the facilities of the HyperChem package and the crystallographic co-ordinates of CsA at PDB 1m63 chain D were taken as a template. To select this experimental X-ray data as a template, we took into consideration many previous findings. On the one hand, the existence of X-ray structures of CsA analogues bound to hCypA18 shed light on the putative bound conformations, and the binding modes all show very similar to CsA bounding form [34]. On the other hand, the water-soluble ligands showed a preferred conformation in water similar to those forming cyclophilin–ligand complexes [32]. Additionally, it has been demonstrated that the preferred conformations of CsA when it is alone in a crystal or in a non-polar solvent and that of CsA bound to a hCyP18 are substantially different [32]. Consequently, the free conformation could not be an indication of the preferred bound conformation.

An alternative to the modeling using crystallographic data of complexes as templates, could be the construction of a model in an aqueous solvent, and then to perform a flexible docking to

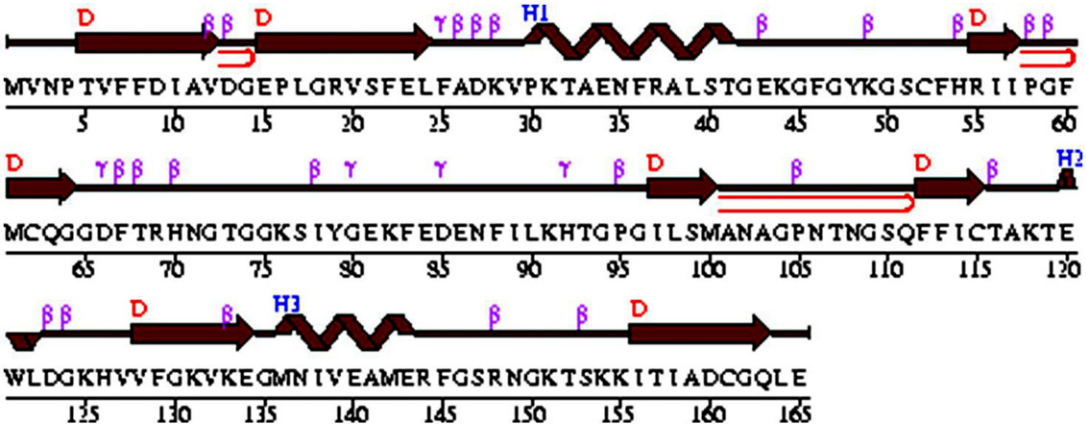

Fig. 2. Graphic display of secondary structure of 1m63C and modelled CyPM proteins. Secondary structure includes one sheet (named D) with 8 strands, 3 helices (H1, H2 and H3), 5 gamma turns, 22 beta turns, 6 beta bulges and 3 beta hairpins. The modelled *Tc*CyP19 shows basically the same secondary structure. This figure was extracted from the PDB web site http://www.rcsb.org/pdb.

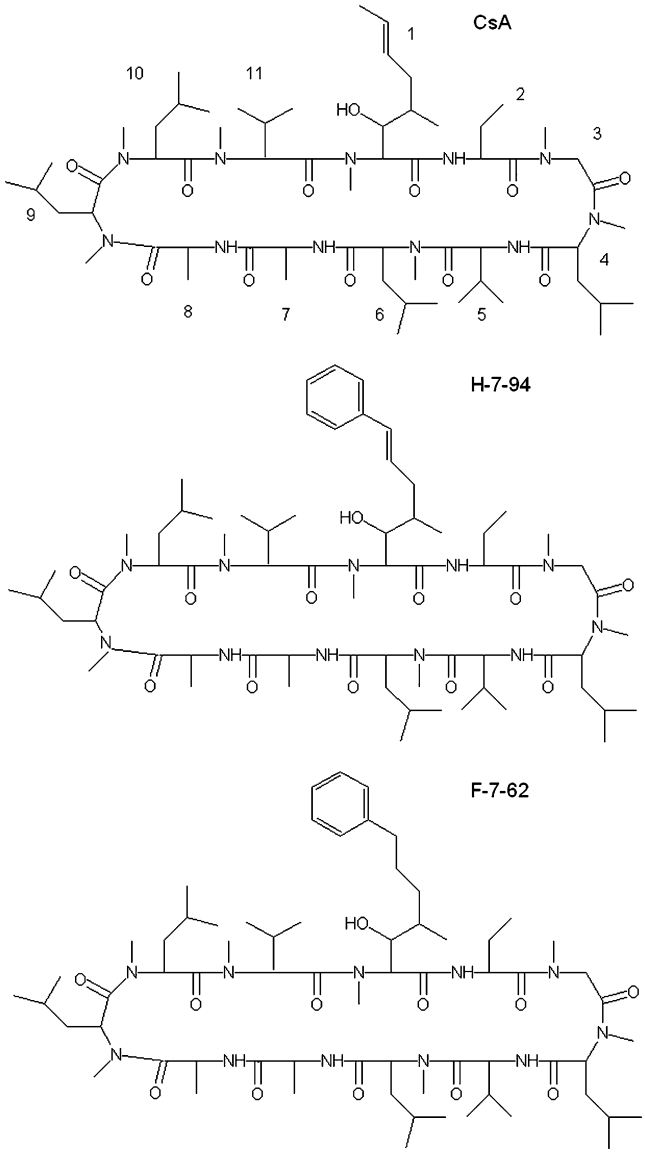

Fig. 3. CsA, H-7-94 and F-7-62 structures. Following the numeration in the CsA structure, the sequence's residues are MeBmt-Abu-Sar-MeLeu-Val-MeLeu-Ala-D-Ala-MeLeu-MeLeu-MeVal. Note that they are unusual amino acids: MeBmt, 4*R*-4-[(*E*)-2-buteny]-4,*N*-dimethyl-L-threonine; Abu, L-α-aminobutyric acid; Sar, sarcosine; MeLeu, *N*-methylleucine and MeVal, *N*-methylvaline. The H-7-94, which common name is (7-phenyl) (7-desmethyl) MeBmt-1-cyclosporine (6,7 *trans* double bond) has only one structural change with respect to CsA: a replacement of a methyl group by a phenyl moiety in the MeBmt residue. H-7-94 and F-7-62 ((7-phenyl)-6,7-dihydro-(7-desmethyl)-MeBmt-1-cyclosporin) differ only in a double bond.

obtain the most stable ligand conformations. However, the docking algorithms demand as initial setting some premises as the binding region (that is in fact one of the results that we would like to obtain) and they are to a great extent dependent on the used score function. In consequence, we decided that, in view of available experimental data (template, K_i, etc.) and having the possibility of making long-term molecular simulations, this technique would be the most adequate: a molecular dynamics simulation such as ours takes into account the flexibility of ligands and the solvent effects allow us to have results consistent with experimental findings.

The graphic analysis and control of possible atom clashes in the different primary models were performed using Swiss-PdbViewer program, and indicated a satisfactory procedure up to this step.

The comparison of *Tc*CyP19 with 1m63C secondary structures only yields a difference due to the inserted loop in *Tc*CyP19 between residue 88 and 89 of the hCyp18 sequence. A view of a three-dimensional structure of 1m63C crystal and the modelled structure of trypanosomal protein is shown in Fig. 4.

The final system models, which were obtained after energy minimisation and molecular dynamic procedures, according with the description in Section 2, are composed of 1682–1741 solute atoms, 9–11 sodium ions, 10–12 chloride ions, and 3069–3222 water molecules, depending of the complex considered.

3.3. Quality of the models

The quality of the main-chain and the side-chain parameters of modelled *Tc*CyP19 and CyPM were evaluated by means of PROCHECK. Table 1 summarizes the results for *Tc*CyP19. In order to compare results, the same analysis was performed for the 1m63C crystal structure (data not show), which were little different. All parameters seemed satisfactory.

The final complex model qualities were evaluated by means of their graphic displays (using Swiss-PDBViewer and VMD, an example is showed in Fig. 5), and rmsd evaluation. The result indicated a great similitude between the modelled *Tc*CyP19 chains of different complexes. Small values of rmsd, lower than or equal to 0.08 and 0.1 $Å^2$ when were taken as reference CA atoms and the backbone or all non-H atoms, respectively, allowed us to quantify such similitude.

Table 2 summarizes the rmsd between each one of these chains and the 1m63C crystallographic data. All rmsd calculated over ligand's CA were lower than 0.09 $Å^2$ and for all identical atoms the value was of 0.14 $Å^2$.

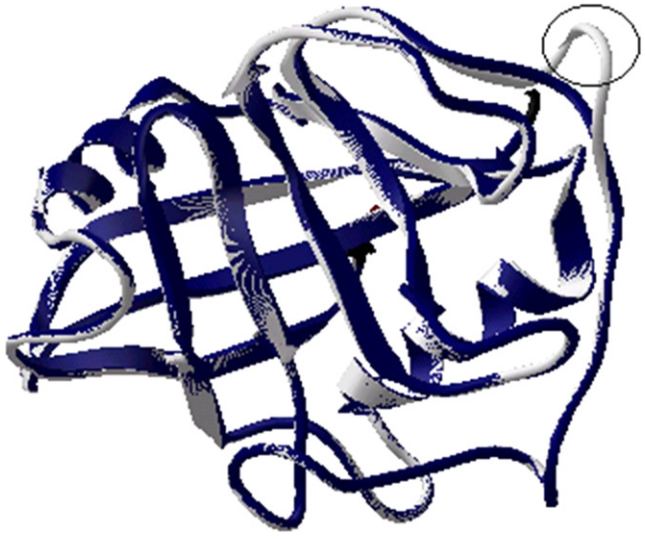

Fig. 4. Graphic superposition of 1m63C (black) and the modelled *Tc*CyP19 (gray). The major difference is the loop due the insertion of A, G and K in *Tc*CyP19 with respect to 1m63C (indicated with a drawing circle).

Table 1
Quality of main-chain and side-chain parameters of modelled *Tc*CyP19

Stereochemical parameter	No. of data points	Parameter value	Typical value	Band width	No. of band widths from mean
Stereochemistry of main-chain					
% residues in A, B, L	132	77.3	82.6	10	−0.5
Omega angle S.D.	164	4.1	6	3	−0.6
Bad contacts/100 residues	0	0	5.2	10	−0.5
Zeta angle S.D.	140	1.7	3.1	1.6	−0.9
H-bond energy S.D.	100	0.7	0.8	0.2	−0.4
Overall G-factor	165	0	−0.4	0.3	1.3
Stereochemistry of side-chain					
Chi-1 *gauche* minus S.D.	35	7.6	19	6.5	−1.8
Chi-1 *trans* S.D.	33	13.4	19.7	5.3	−1.2
Chi-1 *gauche* plus S.D.	51	12.9	18.3	4.9	−1.1
Chi-1 pooled S.D.	119	11.9	18.9	4.8	−1.5
Chi-2 *trans* S.D.	34	17	20.9	5	−0.8

The model was verified at 2.1 Å resolution. A, B, L regions refer to percentage of residues in most favoured regions of Ramachandran plot. Omega angles are torsion angles of protein structure. The parameter value in table represents observed value for *Tc*CyP19 model compared with typical value obtained for well-refined structures at same resolution.

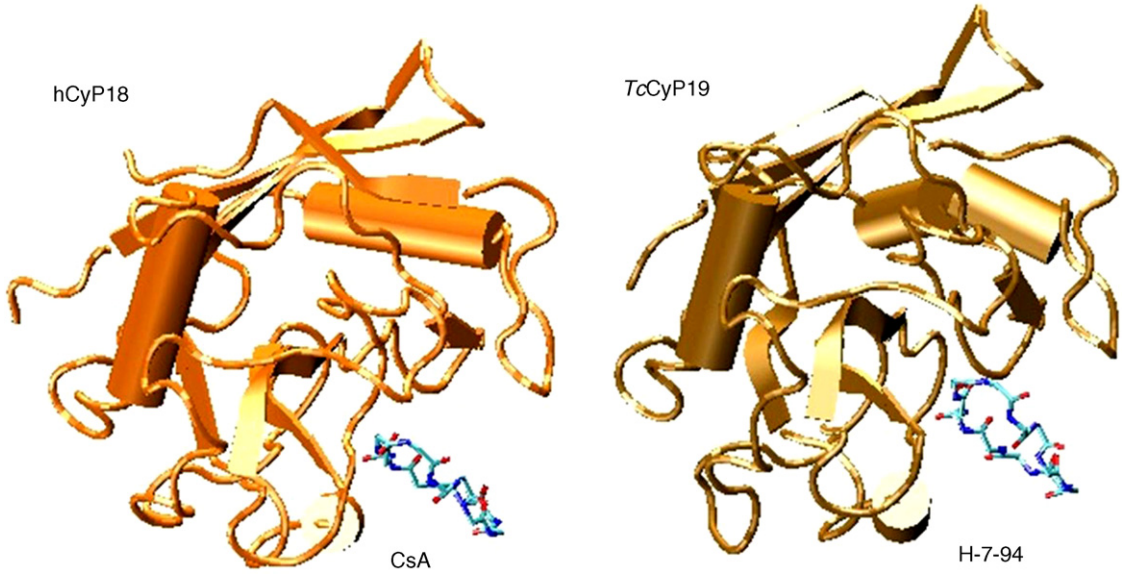

Fig. 5. Diagrams of complex models of hCyP18 and CsA (left) and H-7-94 and *Tc*Cyp19 (right). Only backbone atoms are shown for the ligands.

These assessments allowed us to conclude that the quality of the models obtained justifies its use in further molecular dynamics simulations and evaluations of the relationships of the structures obtained here and their associated properties with experimental biological inhibition on parasite and enzymatic activity results.

Table 2
rmsd between protein chains from different complexes and protein chain from 1m63C

Complex	CA	Backbone	All not H
CsA–hCyP18	0.07	0.11	0.12
F-7-62–hCyP18	0.08	0.11	0.12
H-7-94–hCyP18	0.08	0.11	0.12
CsA–CypM	0.07	0.11	0.12[a]
CsA–*Tc*CyP19	0.15[b]	0.16[b]	0.23[c]

[a] Over all residues excluding Trp(Phe) 121.
[b] Over corresponding residues save inserted or deleted residues (A87, G88, K89 and M1 and V2).
[c] Over only conserved residues.

3.4. Analysis of the interaction between protein and ligands in building models

The putative hydrogen bonds between the ligand and the protein or within the ligand for the different complexes are shown in Table 3. They were evaluated using the analysis program PROCHB incorporated into GROMOS package with the options referred in the table.

The substitution of W121 to F121 in CyPM eliminated the hydrogen bond between the MeLeu9 and the ligand in accordance with the bibliography reports [33]. This further analysis indicated this bond is not substituted for another, for example water. The change of R148 to Q149 in *Tc*CyP19 (that has a shorter side-chain) eliminated a hydrogen bond.

Table 3
Hydrogen bonds in final building models

	CsA–1m 63C	CsA–h CyP18	CsA–Cy PM	F-7-62–h CyP18	H-7-94–h CyP18	CsA–*Tc* CyP19	F-7-62–*Tc* CyP19	H-7-94–*Tc* CyP19
MeBmt(or analog)–MeLeu4	+	+	+	+	+	+	+	+
D-Ala–R148(Q149)	+	+	+	+	+	−	−	−
MeLeu9–W121 (W122/F121)	+	+	−	+	+	+	+	+
MeLeu10–R55(R53)	+	+	+	+	+	+	+	+
Abu–N102 (N103)	−	+	+	+	−	−	+	−

This analysis was performed with the program PROCHB incorporated to GROMOS package setting the maximum distance H atom–acceptor atom equal to 2.5 Å and the minimum angle donor atom–H atom–acceptor atom equal to 135°. The corresponding residues in *Tc*CyP19 or CyPM proteins are shown into parenthesis. Analog refer to (7-phenyl)(7-desmethyl)MeBmt or (7-phenyl)-6,7-dihydro-(7-desmethyl)MeBmt. The first column was included for comparison with H-bonds found in the crystallographic structure.

Failure to find a hydrogen bond between Abu and N102 (or N103), is a consequence of setting the cut-off angle at 135°, since the hydrogen bond was present with a slightly lower angle. Diachronic analyses, obtained by means of the molecular dynamics approach, could be more conclusive in this respect than synchronic analyses of static models.

An increased number of contact atoms at less than 3.7 Å between protein and ligand (Tables 4 and 5) has been observed due to the presence of an aromatic ring in the analogues respect the original MeBmt CsA residue. This aromatic ring interacts with A103 (A104) and to a lesser degree with G104 (G105). The change of R148 for Q149, a shorter side-chain residue, in *Tc*Cyp19 respect hCyP18 drives a loss of interaction (with D-ALA). All catalytic residues, with the exception of M61 (M59) and in some case of L122 (L123), make contacts at less than 3.7 Å with the ligands. Notably, there is not good correlation between these numbers of contacts and inhibitory activity of ligands. Note that a difference of about 7 in the total number of contacts is not significant (this is the difference found between the complex model of CsA–hCyP18 and the 1m63 chain C crystallographic data). Fig. 6 shows in detail the interaction zone for two representative complexes.

3.5. Molecular dynamics

3.5.1. Energetic analysis

The visual inspection of Fig. 7 shows a quick evolution of energy to a constant level with small oscillations.

In a complementary way, data statistical tests were performed. If the system is in equilibrium for a certain period of time, the mean-total energy value over this period cannot be significantly different from the one calculated over the last 100 ps of trajectory. The average value was compared between 0 and 1000, 100 and 1000, 200 and 1000...800 and 1000 periods and 900 and 1000 period. The hypothesis was that if the equilibrium was reached at a given time x, the average at any period $x - 1000$ would not be significantly different from that obtained at the last time period (900–1000 ps). The t-test was performed with a signification level (α) of 0.05 and the null hypothesis (the equality of average) was not rejected for all systems from the 200 ps. The use of t-test allows, in this case, for a less subjective evaluation of system stabilization than that carried out by visual inspection of energy or temperature evolution through the simulation time. This is a simpler and more direct way of making the evaluation than introducing additional suppositions that could be necessary when using

Table 4
Number of contacts between residue ligands and proteins

	CsA–1m 63C	CsA–h CyP18	CsA–Cy PM	F-7-62–h CyP18	H-7-94–h CyP18	CsA–*Tc* CyP19	F-7-62–*Tc* CyP19	H-7-94–*Tc* CyP19
MeBmt (or analog)	12	13	12	29	28	12	30	29
Abu	19	17	18	17	19	19	18	19
Sar	2	2	2	2	3	3	3	3
MeLeu4	0	0	0	0	0	0	0	0
Val	2	2	2	2	2	2	2	2
MeLeu6	0	0	0	0	0	0	0	0
Ala	0	0	0	0	0	0	0	0
D-Ala	4	3	3	4	4	0	0	0
MeLeu9	15	14	17	16	15	13	14	11
MeLeu10	19	16	18	18	18	21	18	20
MeVal	18	17	19	15	19	18	21	19
Total	91	84	91	103	108	88	106	103

The contacts were evaluated at atom distances less than 3.7 Å. This calculation includes all polar hydrogen atoms.

Table 5
Number of contacts between proteins and ligands

Residue in hCyP18 or CyPM	Residue in *Tc* CyP19	Complex							
		CsA–1m63C	CsA–hCyP18	CsA–CyPM	F-7-62–hCyP18	H-7-94–hCyP18	CsA–*Tc*CyPp19	F-7-62–*Tc*CyP19	H-7-94–*Tc*CyP19
A101	A102	1	3	3	2	2	1	3	3
A103	A104	2	2	2	18	18	2	18	18
R148	Q149	7	6	6	7	7	0	0	0
R55	R53	18	15	17	15	16	17	19	19
N102	N103	11	10	11	10	11	11	11	11
Q111	Q112	7	6	6	5	7	7	5	6
Q63	Q61	12	13	13	12	10	13	13	12
G104	G105	0	0	0	2	2	0	2	2
G72	G70	6	5	5	5	7	7	7	7
H126	H127	3	3	3	3	3	3	3	2
L122	L123	1	0	0	0	1	1	1	0
F113	F114	2	3	4	2	4	2	2	2
F60	F58	13	11	12	14	13	15	14	14
W121 (F121)	W122	8	7	9	8	7	9	8	7
Total		91	84	91	103	108	88	106	103

The contacts were evaluated at atom distances less than 3.7 Å. This calculation includes all hydrogen polar atoms.

other techniques such as time-series techniques (i.e. the time correlation function calculations).

The analysis of the relationships between the different energetic calculated terms –Tables 6 and 7 – (that included others like ligand residue interaction with protein, data not shown) and the known stability of different complexes (reflected in the measured IC_{50}) indicated only good primary correlation when the calculated potential complex energy was taken into account. This means that the potential complex energy of the CsA–CyPM is larger than the potential complex energy of the more stable CsA–hCyP18 complex, and the potential complex energy of the CsA–*Tc*CyP19, F-7-62–*Tc*CyP19 and H-7-94–*Tc*CyP19 resulted in the stability complex order. Due to the sequence differences between *Tc*CyP19 and hCyP18, it is not possible to compare this energetic magnitude between *Tc*CyP19's complexes and hCyP18's complexes. Rigour in the study of the significance of the differences between the obtained average potential complex energy for the different complexes demanded that some *t*-test statistical analyses were performed, resulting in significantly different average values ($p \ll 0.001$).

The analysis of the relationships between the potential complex energy and the experimental evidences (Fig. 8) showed a linear correlation. The slopes for the inhibition on the trypomastigote lysis and the epimastigote growth were similar albeit significantly different from the inhibitory *Tc*CyP19

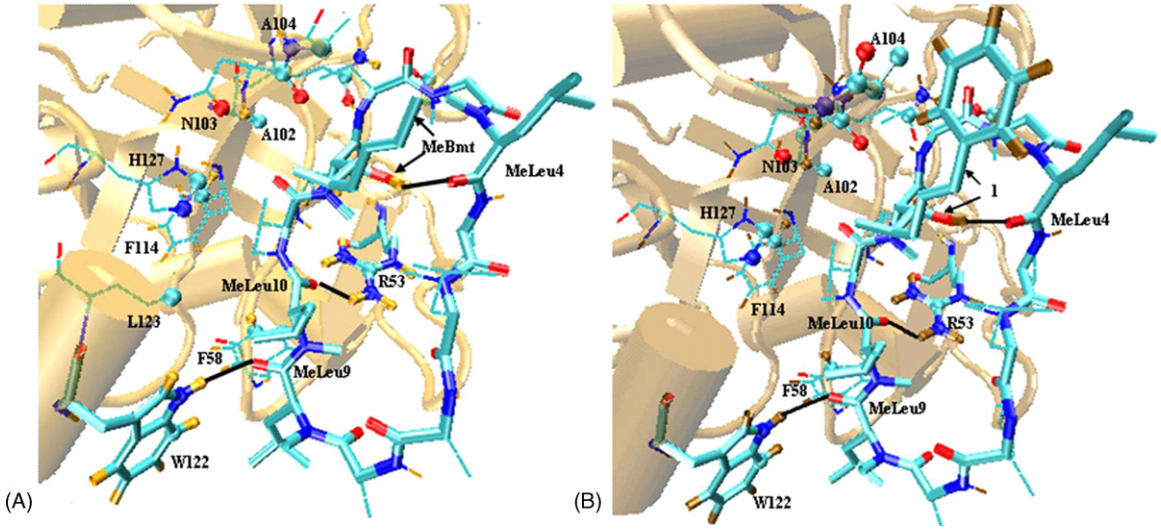

Fig. 6. View of CsA–*Tc*CyP19 (A) and H-7-94–*Tc*CyP19 (B) complexes showing details of the interaction zones. Black rods: H-bonds; thin lines: ligand side-chains and protein residues at distances <3.7 Å. The contacting atoms were shown as balls and CPK graphic models. In thick lines were highlighted CsA and H-7-94 and protein residues making H-bonds. *Tc*CyP19 backbone is showed as a "cartoon" graphic model. The label "1" in H-7-94–*Tc*CyP19 refers to the conventional first ligand residue (7-phenyl)(7-desmethyl)MeBmt.

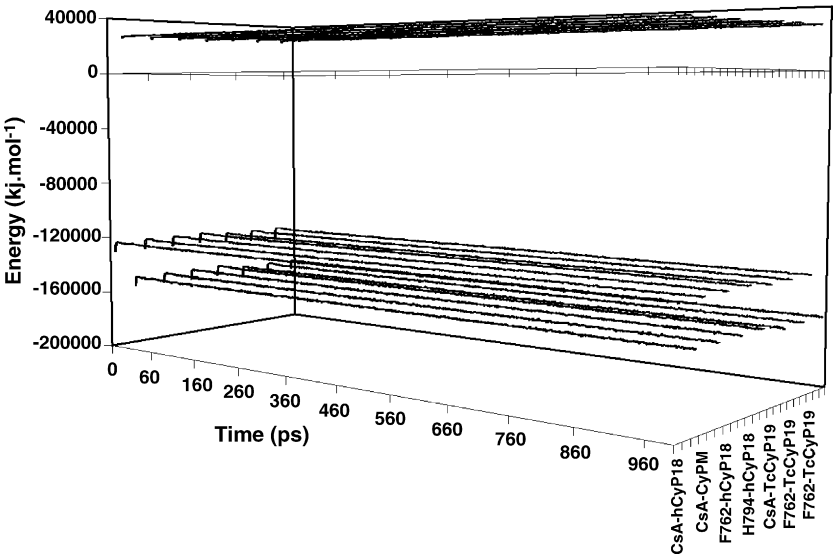

Fig. 7. Energy behaviours of the seven systems submitted to molecular dynamics. The bottom lines represent the potential energy, the middle lines the total energy and the top lines the kinetic energy.

enzymatic activity. The difference in the slopes be justified by taking into account other effects such as transport effects, including membrane barriers, or any binding to another protein.

3.5.2. Structural deviations

The most common measurement of the structural deviations registered through all the simulation time is done by calculating the root mean square deviation (rmsd) parameter. Small structural changes are detected even if they do not have different energies [17]. They are very useful to show average structural motions in different regions of the molecular system or to the evaluation of the relative motion of ligand with respect to the protein to mention two of more common applications.

Analyses of structural deviation along the molecular dynamic trajectories were made by means of the root mean square deviations (rmsd) and the graphic analysis of the obtained structures each 50 ps.

The rmsd were calculated with respect to the final molecular building model co-ordinates (time 0 of molecular dynamic trajectories). When the molecular fittings were performed taking into account all alpha carbons, the rmsd showed for all complexes a maximum for the alpha carbon of 1.6 and 2.2 Å^2

Table 6
Summary of the principal whole energetic values calculated on the 500–1000 ps period of the MD (kJ mol^{-1})

	CsA–h CyP18	CsA–Cy PM	F-7-62–h CyP18	H-7-94–h CyP18	CsA–*Tc* CyP19	F-7-62–*Tc* CyP19	H-7-94–*Tc* CyP19
Total energy	−124,349	−124,375	−124,084	−123,996	−126,101	−126,057	−125,986
Kinetic energy	27,497	27,476	27,450	27,453	28,464	28,473	28,467
Potential energy	−151,846	−151,851	−151,534	−151,448	−154,565	−154,530	−154,453
Potential covalent energy	4,983	5,014	5,004	5,014	4,842	4,897	4,884
Potential no covalent energy	−156,828	−156,866	−156,538	−156,462	−159,407	−159,427	−159,338
Potential complex energy	−25,702	−25,547	−25,876	−25,970	−22,199	−22,291	−22,442
Potential no covalent complex energy	−30,684	−30,561	−30,880	−30,983	−27,042	−27,188	−27,326

The majority of items explain itself. The potential complex energy was calculated by taking the total potential energy and deducting the potential energy of interaction between all the solvent molecules, the chlorine and the sodium ions.

Table 7
Summary of the main energetic values referred to the different ligand without covalent interaction, calculated on the MD 500–1000 ps period (kJ mol^{-1})

	CsA–h CyP18	CsA–Cy PM	F-7-62–h CyP18	H-7-94–h CyP18	CsA–*Tc* CyP19	F-7-62–*Tc* CyP19	H-7-94–*Tc* CyP19
Ligand–protein	−315	−286	−334	−297	−258	−330	−297
Ligand–solvent	−361	−381	−376	−393	−382	−382	−406
Ligand–surrounding	−676	−667	−710	−690	−640	−712	−703
Total ligand	−776	−784	−799	−788	−764	−819	−818

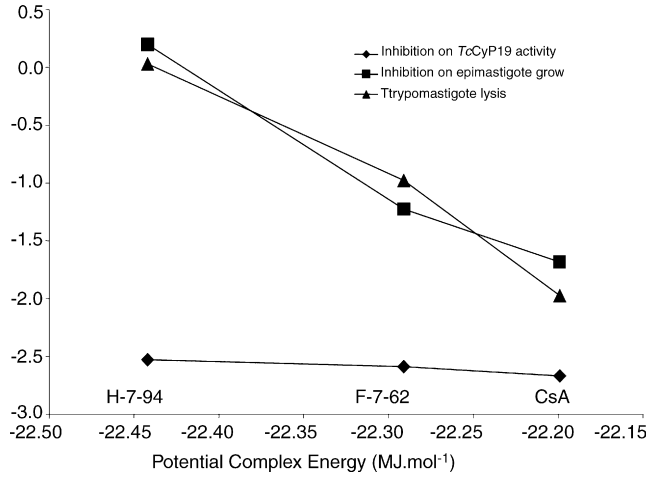

Fig. 8. Graphic representation of the relationships between the potential complex energy and the inhibition concentration of the three compounds assayed on *Tc*CyP19 and on the parasite. The values in the *Y*-axis are expressed as the natural logarithm of the inverse of IC_{50}.

for all atoms except H. To obtain an idea about the structural deviations of protein components of the complexes, analog structural fitting and rmsd calculations were performed only on protein atoms, showing maximum values of 1.6 and 2.2 Å^2, respectively. The same procedure for ligands gave maximum values of 1.3 and 1.9 Å^2, respectively. Finally, to obtain some measures of the relative ligand motions with respect to the protein chain, the rmsd were calculated for alpha-carbon atoms or for all heavy atoms of ligands, taking the molecular fittings only over the alpha protein carbons. In all cases, the maximum rmsd values obtained were 3.3 and 3.7 Å^2, respectively, corresponding to stable systems.

3.5.3. Atomic contacts between protein and ligands

Tables 8 and 9 summarize the average of atomic contacts between protein and ligands. The total number of contacts drops when compared to the corresponding total number of contacts in the models. This is to be expected, due to the incorporation of kinetic energy in molecular dynamic simulation over the minimized energetic models allows some relaxation, and the distances could increase in the weakest interactions. In this sense, the MeBmt (or its structural modifications in H-7-94 or F-7-62) and MeLeu10 show various weak interactions in the models. On the other hand, MeLeu9 shows an increase of interaction numbers in all complexes except CsA–CyPM, most likely because of the absence of hydrogen bonding that links these residues in other complexes.

The total number of contacts showed a general correlation with the ligand–protein interaction energies (showed in Table 7), but, there was not a good correlation with the measured ligand–protein affinity (when it was available).

Like in the starting models, the substitution of a methyl moiety for the MeBmt side-chain to the more voluminous phenyl one in the CsA analogs drives an increase of number of contacts, particularly due to new interactions with A103 in hCyP18 or A104 in *Tc*CyP19.

All catalytic residues, with the exception of G70 in CsA–*Tc*CyP19 and L123 in H-7-94–*Tc*CyP19, make contacts at less than 3.7 Å with the ligands.

The molecular dynamics simulation shows the interaction loss of R148 in hCyP18 with ligand: the interaction is so weak that it allows the side-chain to move away the ligand; this is observed in the molecular dynamic graphic analysis of the complexes too.

3.5.4. Hydrogen bonds analysis

The occurrence percentages of hydrogen bonds between the ligand and the protein or within the ligand for the different complexes taking the last 500 conformations of the molecular dynamic trajectories are presented in Table 10. This table includes only hydrogen bonds which have more than or equal 50% of occurrence in any complex. For comparative purposes, please refer to Table 3 to see identified hydrogen bonds. The minimum limit of occurrence of 50% of an H-bond was considered good enough to detect the presence of an H-bond; all others alleged hydrogen bonds showed an occurrence of less than 10%, with two exceptions for the CsA–CyPM complex: SAR–R55 (13%) and MeVal–Q102 (40%). The significance of

Table 8
Average of ligand–protein contacts for ligand residues

	CsA–h CyP18	CsA–Cy pM	F-7-62–h CyP18	H-7-94–h CyP18	CsA–*Tc* CyP19	F-7-62–*Tc* CyP19	H-7-94–*Tc* CyP19
MeBmt (or analog)	8	13	19	15	4	20	13
Abu	14	7	19	16	14	20	14
Sar	5	12	2	2	1	2	2
MeLeu 4	2	2	0	0	0	1	0
Val	4	2	3	2	1	1	3
MeLeu6	0	0	0	0	0	0	0
Ala	0	0	0	0	0	0	0
D-Ala	1	1	0	0	0	0	0
MeLeu9	22	14	19	20	18	16	17
MeLeu10	9	0	5	6	6	1	6
MeVal	14	12	14	15	16	13	12
Total	80	62	82	77	61	74	68

The average take account the atomic contacts at less than 3.7 Å finding in the modelled complexes over the 500–1000 ps time molecular dynamic simulation. The calculation was performed over 11 structures – each 50 ps – and includes all hydrogen polar atoms.

Table 9
Average of ligand–protein contacts for protein residues

Residue in hCyp18 or CypM	Residue in *Tc* CyP19	CsA–h CyP18	CsA–Cy pM	F-7-62–h CyP18	H-7-94–h CyP18	CsA–*Tc* CyP19	F-7-62–*Tc* CyP19	H-7-94–*Tc* CyP19
A101	A102	1	5	3	3	2	2	2
A103	A104	3	3	9	12	4	9	7
R148	Q149	2	0	0	0	0	0	0
R55	R53	15	5	6	4	2	4	4
N102	N103	10	13	9	9	8	10	10
N149	T150	0	1	0	0	0	0	0
Q111	Q112	2	3	2	4	1	4	4
Q63	Q61	2	7	7	3	1	8	4
G104	G105	0	0	3	1	0	2	2
G72	G70	3	6	2	1	0	1	1
H126	H127	2	2	2	2	3	1	2
I57	I55	0	1	0	0	0	0	0
L122	L123	1	1	1	1	1	1	0
K82	K80	0	0	0	0	1	0	1
M61	M59	1	1	1	1	1	1	1
F113	F114	4	2	6	3	6	6	4
F60	F58	22	4	15	17	17	7	15
P105	P106	0	0	1	0	0	2	0
T73	T71	3	1	4	3	4	5	1
W121 (F121)	W122	9	10	11	12	10	11	10
Total		80	62	82	77	61	74	68

The average take into account the atomic contacts at less than 3.7 Å found in the modelled complexes over the 500–1000 ps time molecular dynamic simulation. The calculation was performed over 11 structures – each 50 ps – and includes all hydrogen polar atoms.

the MeLeu9–W122 hydrogen bond in H-7-94–*Tc*CyP19 was further evaluated, due to the borderline value of it occurrence. For example, if the last 100 ps of molecular dynamic simulation time was considered, this H-bond was detected in the 54% of structures.

In all cases an intra-ligand hydrogen bond is shown, between MeBmt (or analogs) and MeLeu4. It is formed by the OH of MeBmt (or analog) group and the carbonilic oxygen of MeLeu4.

An hydrogen bond in F-7-62 complexes appears between the (7-phenyl)-6,7-dihydro-(7-desmethyl)MeBmt and Q63 (or Q61). The acceptor atom is the carbonilic oxygen of the F-7-62 residue, and the donor atom the side-chain nitrogen of Q.

The hydrogen bond over MeLeu9, critical in the CsA–hCyP18 interaction, was clearly detected through the simulation of all complexes except in CsA–CyPM and, surprisingly, in CsA–*Tc*CyP19. In the CsA–CyPM model, there is no H-bond due to the presence of a Phe, which substitutes the Trp. Then, in the case of CsA–CypM, the H-bond absence could trigger a rearrangement leading to a reduction in the total complex energy (and the total number of H-bonds in the interaction zone), that could justify the corresponding decrease in the CsA–CypM experimental binding. In the case of CsA–*Tc*CyP19 model, in which no equivalent H-bond was significantly detected, the effect of a rearrangement could foster a binding strong enough to maintain the stability of the complex. The energy of the ligand–protein interaction, which is more stabilizing for CsA–CyPM than for CsA–TcCyP19 complex (Table 7) illustrates that the stabilizing interactions could take place not only in the closer ligand neighbourhood but could also compromise distant zones of the entire protein structure.

Table 10
Percentages of hydrogen bonds occurrence throughout the last 500 ps trajectory molecular dynamic time

	CsA–h CyP18	CsA–Cy pM	F-7-62–h CyP18	H-7-94–h CyP18	CsA–*Tc* CyP19	F-7-62–*Tc* CyP19	H-7-94–*Tc* CyP19
MeBmt (or analog)–MeLeu4	93	82	90	89	96	82	92
D-Ala–R148 (Q149)	1	0	0	0	0	0	0
MeLeu9–W121 (W122 or F121)	55	0	66	55	24	62	50
MeLeu10–R55 (R53)	7	0	0	0	0	0	0
Abu–N102 (N103)	96	0	42	38	87	75	79
MeBmt (or analog)–Q63 (Q61)	0	4	64	11	0	82	34
Total	3	1	3	2	2	4	3

This analysis was performed with the program PROAHB within the GROMOS package with the options: maximum distance H atom–acceptor atom of 2.5 Å and minimum angle donor atom–H atom–acceptor atom of 135°. The percents are calculated over 500 co-ordinate file (each picosecond). Total row: the sum of the number of hydrogen bond that appears over or equal 50%. The corresponding residues in the ligand or *Tc*CyP19 or CyPM protein are indicated between parentheses.

Table 11
Energetic evaluation of interaction MeLeu9–Trp121 (or Trp122) (kJ mol^{-1})

	CsA–h CyP18	CsA–Cy PM	F-7-62–h CyP18	H-7-94–h CyP18	CsA–*Tc* CyP19	F-7-62–*Tc* CyP19	H-7-94–*Tc* CyP19
Interaction energy between residues	−20.1	−10.7	−23.7	−22.6	−16.7	−23.5	−24.9
Difference between all atoms in the MeLeu and Trp residues respect to CsA–hCyP18 complex	0	9.4	−3.6	−2.5	3.4	−3.4	−4.8
Difference of interaction energy of H–O with respect to CsA–hCyP18 complex	0	Not correspond	−4.2	−2.0	3.2	−4.1	−5.6

The values of first and second row are the average of the last 500 ps. The values of the last row were averaged over the last 100 ps.

Additionally, we calculated the interaction energies between MeLeu9 and Trp121 (or Trp 122) residues. We selected the 900 ps structures for each model and we run a short 100 ps MD to collect data in order to sense the kind and strength of interactions. Table 11 shows a significant decrease in the strength of the interactions between both residues in the complex CsA–TcCyP19. The decrease is greatest for the CsACyPM case. A similar conclusion was reached when we calculated the specific interaction between H and O in the couple MeLeu9–Trp121 (122) in the different complexes (third row in Table 11). Moreover, by means of this procedure, we are demonstrating that the biggest component in the differences of residue interactions in the studies of complexes is the H–O interaction.

The analysis of a dynamic trajectory of a molecule structure gives different information from that obtained from the models, as shown in the Sections 3 and 4. This analysis involves a significant number of allowed molecular conformations and this is more conclusive than the circumstantial picture given by just one particular model configuration. In fact, according to this analysis, the initially detected hydrogen bonds between the D-Ala and R148 and between MeLeu10 and R55 (or R53), shown in Table 4, were not significant, taking into account the low frequency at which it appeared throughout the simulation.

3.5.5. Graphic analysis of simulation

The graphic visualization of the complex conformations during the simulation time did not show a relevant distortion in the shape of the complex (two representative examples are shown in Fig. 9). A global oscillating movement of the structure centred around its own stable structure was observed. This visualization indicated that the equilibrium was reached from 200 ps on, a result that agrees with the equality of mean energies and with the rmsd structural analysis from this time. However, the need to obtain a representative sampling with a large number of conformations, and simultaneously to be certain that an equilibrated system is being analysed, led us to be more demanding and to start the analysis from 500 ps.

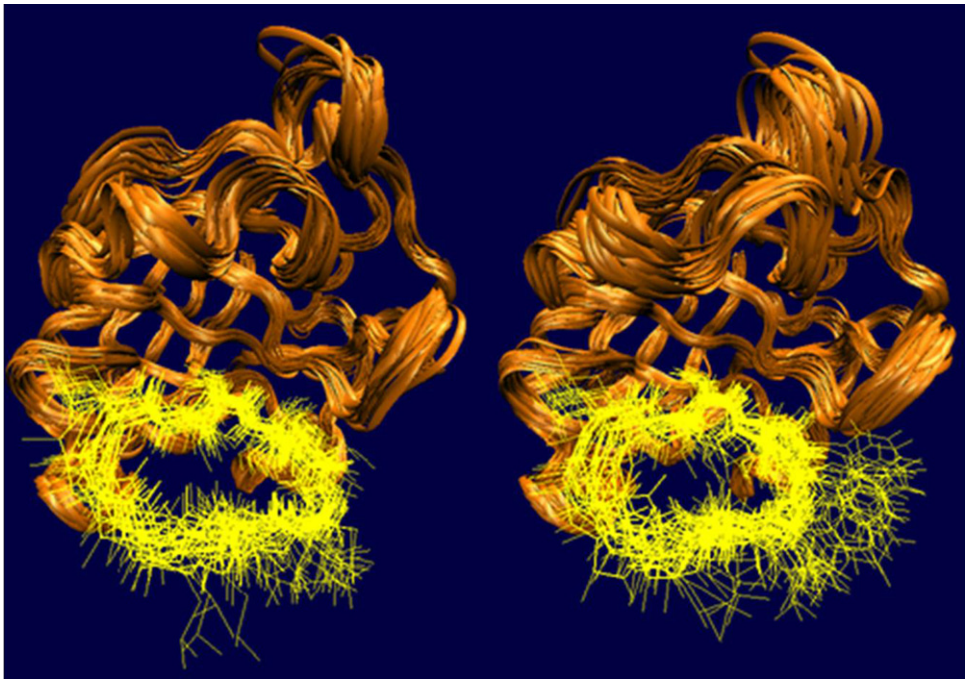

Fig. 9. CsA–*Tc*CyP19 and H-7-94–*Tc*CyP19 complexes simulated through 1 ns, each 50 ps, overlapping in such way 22 images. The proteins are represented by ribbons. The ligands are represented by thin yellow lines of theirs atomic bonds.

4. Conclusions

The evaluated quality of models was satisfactory enough to ensure the further use of these models to investigate the ligand–protein interactions. A high sequence identity between template and modelled proteins, the Procheck results, the graphic analysis, and the rmsd evaluation on the modelled complexes led us to this conclusion, reinforced by the observation of stability in the energies and structures shown throughout all molecular dynamics simulations.

Comparison of the dynamic behaviour of the CsA–hCyP18, CsA–*Tc*CyP19 and CsA–CyPM complexes, leads to the conclusion that the H-bond between the residues Trp121 in the hCyP18, Trp122 in the *Tc*Cyp19 and the ligands was not essential.

Of all calculated energetic values, the potential complex energy was the only magnitude that correlated with a clear linear relationship with both PPIase activity inhibition and parasitic inhibitory effects. This suggests that for these biological systems, changes in the total atomic interactions, even those that are far from the interaction site, foster this protein–ligand binding.

Finally, the designed strategy which implies model building, quality evaluation, molecular dynamics procedures, and energy interaction calculations was appropriate to ascertain the relationships between experimental evidence and calculated magnitudes.

Acknowledgements

This work was supported by the NASA/ChagaSpace network. JB and AMR are members of the Research Career of the Consejo Nacional de Investigaciones Científicas y Técnicas (CONICET), Argentina. The authors thank the technical assistance of Prof. Cecilia Rennie in the revision of the manuscript. Prof. José Fuentes (DETEMA—Facultad de Química) was of great support in the statistical analysis.

References

[1] C.M. Morel, Snippets of achievement, Special Programme for Research and Training in Tropical Diseases, 2001, TDR/GEN/0.2001, 1.1.
[2] L. Flohé, R. Radi, M. Paulino, Consensus statement: session 9, Discovery Research and New Therapeutic Tools, Proceedings of the Scientific Working Group Meeting on Chagas Disease, Buenos Aires, Argentina, 2005.
[3] R.E. Handschumacher, M.W. Harding, J. Rice, R.J. Drugge, D.W. Speicher, Cyclophilin: a specific cytosolic binding protein for cyclosporin A, Science 226 (4674) (1984) 544–577.
[4] N. Takahashi, T. Hayano, M. Suzuki, Peptidyl-prolyl *cis–trans* isomerase is the cyclosporin A-binding protein cyclophilin, Nature 337 (6206) (1989) 473–475.
[5] A. Galat, Peptidylprolyl *cis*/*trans* isomerases (immunophilins): biological diversity – targets – functions, Curr. Top. Med. Chem. 3 (12) (2003) 1315–1347.
[6] J. Liu, J.D. Farmer Jr., W.S. Lane, J. Friedman, I. Weissman, S.L. Schreiber, Calcineurin is a common target of cyclophilin–cyclosporin A and FKBP–FK506 complexes, Cell 66 (4) (1991) 807–815.
[7] S. Ho, N. Clipstone, L. Timmermann, J. Northrop, I. Graef, D. Fiorentino, J. Nourse, G.R. Crabtree, The mechanism of action of cyclosporin A and FK506, Clin. Immunol. Immunopathol. 80 (3 Pt 2) (1996) S40–S55.
[8] M. Potenza, A. Galat, T.A. Minning, A.M. Ruiz, R. Duran, R.L. Tarleton, M. Marín, L.E. Fichera, J. Búa, Analysis of the *Trypanosoma cruzi* cyclophilin gene family and identification of Cyclosporin A binding proteins, Parasitology, in press.
[9] J. Bua, L. Aslund, N. Pereyra, G.A. Garcia, E.J. Bontempi, A.M. Ruiz, Characterisation of a cyclophilin isoform in *Trypanosoma cruzi*, FEMS Microbiol. Lett. 200 (1) (2001) 43–47.
[10] A. Bell, H.C. Roberts, L.H. Chappell, The antiparasite effects of cyclosporin A: possible drug targets and clinical applications, Gen. Pharmacol. 27 (6) (1996) 963–971.
[11] R.E. McCabe, J.S. Remington, F.G. Araujo, In vivo and in vitro effects of cyclosporin A on *Trypanosoma cruzi*, Am. J. Trop. Med. Hyg. 34 (5) (1985) 861–865.
[12] J. Bua, A.M. Ruiz, M. Potenza, L.E. Fichera, In vitro anti-parasitic activity of Cyclosporin A analogs on *Trypanosoma cruzi*, Bioorg. Med. Chem. Lett. 14 (18) (2004) 4633–4637.
[13] S. Goldsmith-Fischman, B. Honig, Structural genomics: computational methods for structure analysis, Prot. Sci. 12 (9) (2003) 1813–1821.
[14] P. Bamborough, F.E. Cohen, Modeling protein–ligand complexes, Curr. Opin. Struct. Biol. 6 (2) (1996) 236–241.
[15] H.L. Monaco, M. Rizzi, A. Coda, Structure of a complex of two plasma proteins: transthyretin and retinol-binding protein, Science 268 (5213) (1995) 1039–1041.
[16] O. Tapia, B. Oliva, O. Nilsson, E. Querol, F.X. Avilés, in: E. Girald, D. Andreu (Eds.), ESCOM, Leiden, 1991, p. 581.
[17] M. Paulino, A. Esteves, M. Vega, G. Tabares, R. Ehrlich, O. Tapia, Modelling a 3D structure for EgDf1 from *Echinococcus granulosus*: putative epitopes, phosphorylation motifs and ligand, J. Comput. Aid. Mol. Des. 12 (4) (1998) 351–360.
[18] H.M. Berman, V. Westbrook, Z. Feng, G. Gilliland, T.N. Bhat, H. Weissig, I.N. Shindyalov, P.E. Bourne, The protein data bank, Nucl. Acids Res. 28 (2000) 235–242.
[19] S.F. Altschul, W. Gish, W. Miller, E.W. Myers, D.J. Lipman, Basic local alignment search tool, J. Mol. Biol. 215 (3) (1990) 403–410.
[20] S.B. Needleman, C.D. Wunsch, A general method applicable to the search for similarities in the amino acid sequence of two proteins, J. Mol. Biol. 48 (3) (1970) 443–453.
[21] J.Z. Xiang, Jackal, Columbia University, Howard Hughes Medical Institute, 2002.
[22] HyperChem™, 6.01, Hypercube, Inc., 2000.
[23] N. Guex, M.C. Peitsch, SWISS-MODEL and the Swiss-PdbViewer: an environment for comparative protein modeling, Electrophoresis 18 (15) (1997) 2714–2723.
[24] W.F. van Gunsteren, S.R. Billeter, A.A. Eising, P.H. Hünenberger, P. Krüger, M.A. E., W.R.P. Scott, I.G. Tironi, GROMOS96, Hochschulverlag AG, ETH Zürich, BIOMOS b. v. Zürich, Groningen, 1996.
[25] H.J.C. Berendsen, J.P.M. Postma, W.F. van Gunsteren, J. Hermans, Interaction models for water in relation to protein hydration, in: B. Pullman (Ed.), Intermolecular Forces, Reidel, Dordrecht, 1981, pp. 331–342.
[26] J.P. Ryckaert, G. Ciccotti, H.J.C. Berendsen, Numerical integration of the Cartesian equation of motion of a system with constraints: molecular dynamics of *n*-alkanes, J. Comput. Phys. 23 (1977) 327–341.
[27] W. Humphrey, A. Dalke, K. Schulten, VMD: Visual molecular dynamics, J. Mol. Graph. 14 (1) (1996), 33–38, 27–28.
[28] R.A. Laskowski, M.W. MacArthur, D.S. Moss, J.M. Thornton, PROCHECK: a program to check the stereochemical quality of protein structure, J. Appl. Cryst. 26 (1993) 283–291.
[29] H.J.C. Berendsen, J.P.M. Postma, W.F. van Gunsteren, A. DiNola, J.R. Haak, Molecular dynamics with coupling to an external bath, J. Chem. Phys. 81 (1984) 3684–3690.
[30] O. Nilsson, Molecular conformational space analysis using computer graphics: going beyond FRODO, J. Mol. Graph. 8 (4) (1990) 192–200, 192–200, 212–213.
[31] J. Kallen, V. Mikol, P. Taylor, M.D. Walkinshaw, X-ray structures and analysis of 11 cyclosporin derivatives complexed with cyclophilin A, J. Mol. Biol. 283 (2) (1998) 435–449;
W. Braun, J. Kallen, V. Mikol, M.D. Walkinshaw, K. Wuthrich, Three-

dimensional structure and actions of immunosuppressants and their immunophilins, FASEB J. 9 (1) (1995) 63–72.
[32] P. Taylor, H. Husi, G. Kontopidis, M.D. Walkinshaw, Structures of cyclophilin–ligand complexes, Prog. Biophys. Mol. Biol. 67 (2/3) (1997) 155–181.
[33] J. Liu, C.M. Chen, C.T. Walsh, Human and *Escherichia coli* cyclophilins: sensitivity to inhibition by the immunosuppressant cyclosporin A correlates with a specific tryptophan residue, Biochemistry 30 (9) (1991) 2306–2310.
[34] J. Dornan, P. Taylor, M.D. Walkinshaw, Structures of immunophilins and their ligand complexes, Curr. Top. Med. Chem. 3 (12) (2003) 1392–1409.